Building a Birdcage Resonator for Magnetic Resonance Imaging Studies of CNS Disorders

Michael Lang

Undergraduate Honours Thesis

Advisors: Dr. Chris Bidinosti and Dr. Melanie Martin

University of Winnipeg

Winnipeg, MB Canada

April 20, 2011

Abstract

Magnetic resonance imaging (MRI) studies are currently being performed at the Health Sciences Center (HSC) in Winnipeg in order to understand better central nervous system (CNS) disorders. Using a 7-Tesla MRI system and rodent models of Alzheimer's disease and Multiple Sclerosis, novel MRI techniques are being exploited to enhance the diagnosis of these disorders in all stages of their development. The studies require a variety of small-scale radio frequency (RF) resonators to achieve high quality images of rodents of different sizes. There are currently several sizes of RF resonators available for use at the HSC, but of those, there is not a suitable resonator for rodents between 25 mm and 30 mm in diameter. The purpose of this project is to construct and test a 28.5 mm inner diameter birdcage resonator intended for mice and rats of this size. The newly built resonator is compared to the next availably sized resonator to show the benefit of using RF resonators which are sample-size apropriate. Scans performed on an excised rat brain show that the 28.5 mm resonator provides a higher signal-to-noise ratio (SNR) than the previously used 33 mm resonator. We achieved an SNR of 30.3 with the 28.5 mm resonator compared with an SNR of 21.7 for the 33 mm resonator, clearly indicating that the newly built resonator is better suited for samples of 28.5 mm or less. Higher resolution images can now be acquired from rodents in this size range, leading to finer image details and a better understanding of the CNS disorders being studied.

Acknowledgements

- Chris Bidinosti and Melanie Martin, Thesis Advisors - for suggesting an interesting topic and supporting my efforts with tremendous enthusiasm.

- Jeff Martin, Thesis Committee - for taking time from his busy schedule to provide useful suggestions.

- Vyacheslav Voltovskyy, MR Technology Research Council Officer NRC-IBD - for providing help with design, construction, and understanding of my project with an incredibly positive attitude throughout.

- Jarod Matwiy, MR Technology Technical Officer NRC-IBD - for helping me machine parts and optimize circuitry, and providing immediate assistance under time constraints.

- Brendon Matwiy, MR Technology Technical Officer NRC-IBD - for his assistance machining parts, and general guidance throughout my project's construction.

- Anthony Wessel, MR Technology Technical Officer NRC-IBD - for helping me with equipment and providing useful insight in the workshop and on the electronics bench.

- Richard Buist, Department of Pharmacology and Therapeutics University of Manitoba - for helping me acquire images throughout the course of my project, and explaining a great deal along the way.

- Laryssa Kurzewicz, University of Manitoba Student - for preparation of the rat brain sample, and assistance acquiring images.

- Jonathan Thiessen, University of Manitoba Student - for helping me acquire images and providing Matlab code for SNR calculations.

Contents

List of Figures

1 Introduction

1.1 Purpose of this Project

Alzheimer's disease and Multiple Sclerosis are two central nervous system (CNS) disorders currently under investigation by Dr. Melanie Martin of the Universiy of Winnipeg. Making use of a 7-Tesla Magnetic Resonance Imaging (MRI) scanner system situated at the Health Sciences Center (HSC) in Winnipeg, Dr. Martin and her collaborators are developing novel techniques to diagnose CNS disorders earlier, and follow the progression of the disorders to understand better how they develop. The MRI system being used is not a clinical scanner, and the imaging is focused primarily on rodent models of human CNS disorders. The 7-Tesla system is not as large as a clinical scanner and makes use of smaller pieces of hardware to perform rodent imaging.

In order to perform scans, MRI systems require the use of a radio frequency (RF) resonator, of which there are several varieties. The HSC 7-Tesla system primarily makes use of a particular type of RF resonator known as a birdcage. Due to the nature of RF resonators, it is advantageous to image with one that closely fits the sample, and therefore several birdcage resonators are required by the HSC to perform scans on varying sized mice and rats. Although several sizes are currently among the arsenal at the HSC, there exists a gap at a size required for many of the scans being performed. The purpose of this thesis project is to build an intermediate sized coil to fill in this gap, allowing for high quality images of mice and rats which are between 25 mm and 30 mm in diameter. A comparison will be performed between the new 28.5 mm coil and a 33 mm coil to demonstrate the benefit of using a sample-size appropriate coil.

1.2 Why use Magnetic Resonance Imaging

Although there exist several excellent imaging methods in today's medical community, MRI techniques are gaining popularity and have several advantages making them suitable for CNS studies. MRI is a form of tomographic imaging, like Positron Emission Tomography (PET) and X-ray Computed Tomography (CT). Unlike PET and CT techniques, however, MRI is completely non invasive, requiring no injected contrasting agents and subjecting the sample being imaged to no ionizing radiation. In this sense, MRI is much safer for, and possesses fewer health issues to, the average patient requiring a diagnostic treatment. Modern MRI systems are capable of providing images in any plane through any part of the body, with acquisition in as little as a few minutes and resolutions of less than 1 mm. MRI also produces excellent contrast images which allows for higher sensitivity to different physiological aspects than other imaging methods. For this reason, MRI has its advantages over PET or CT when imaging certain regimes.

Since MRI can be performed on living samples with no adverse affects, longitudinal studies can be carried out on mice and rat models of CNS disorders to observe the progression through the course of the animal's life. This is extremely important for developing diagnosis and treatment methods as repeat and long-term studies are the best method for determining how the disorders change and respond to treatment.

2 Nuclear Magnetic Resonance Basics

Nuclear magnetic resonance (NMR) is the fundamental principle which allows MRI to be performed. This section will discuss the basic details of NMR. For greater detail on this subject, a number of excellent resources are available such as References [1-7].

2.1 Atomic Structure

Atoms consists of a central nucleus with orbiting electrons. The nucleus is made of nucelons which can be divided into two types, protons and neutrons. A positively charged atom results from having a greater number of protons in the nucleus than orbiting electrons. A negatively charged atom is the opposite, in which more orbiting electrons are present when compared to the protons of the nucleus. The atom is electrically stable or neutral when the number of protons equals the number of electrons and the net charge is zero.

Electrons and nucleons possess spin angular momentum – commonly referred to as just "spin" – which can be visualized as an actual physical rotation of the particle about its own axis. Electrons also posess orbital angular momentum. A nucleus will have half-integral spin if it has an odd mass number, zero spin if it has an even mass number and charge number, and integral spin if has an even mass number but an odd charge number [1].

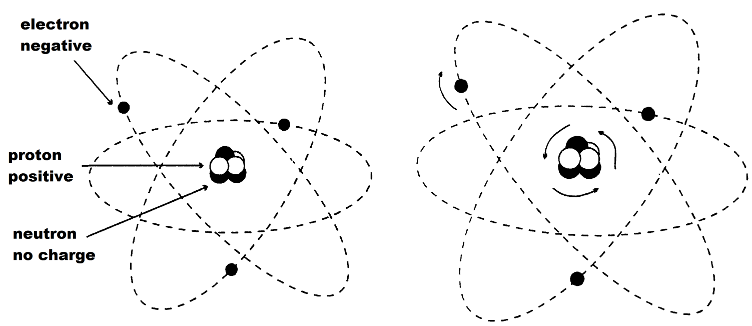

Figure 1: Schematic of the classical model of the atom. (Image from Westbrook [2].)

2.2 Spin and Magnetic Field Interaction

The spin angular momentum **I** posessed by atomic nuclei is in fact a quantum effect. However, viewed classically one can consider nuclei such as hydrogen as a rotating charged sphere producing a magnetic dipole moment and an associated magnetic field. When thought of this way, the hydrogen nucleus is analagous to a microscopic bar magnet [1]. In the presence of an external magnetic field, the nuclear magnetic dipole moment or magnetic moment, represented by the vector quantity μ, will tend to align with the external field lines. When an ensemble of magnetic moments in a sample align in one direction, there exists a net magnetization within the sample.

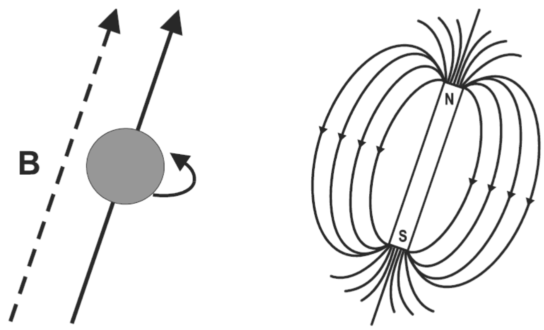

Figure 2: Magnetic moment of a hydrogen nucleus (single proton), compared to a bar magnet (Image from Brown [3].)

The ratio of the magnetic moment μ of a nucleus to its spin $\mathbf{I}$ is called the gyromagnetic ratio:

$$\gamma = \frac{\mu}{I}, \tag{1}$$

where “gyro” refers to the spin, and “magneto” to the magnetic moment of the nuclei.

2.3 Magnetic Resonance Active Nuclei

In nuclear magnetic resonance (NMR), our concern lies with the nucleus of the atom and not with its surrounding electrons. As mentioned, the nucleus of an atom is composed of protons and neutrons, and the configuration of these two types of nucleons dictates whether or not an atom is a suitable candidate for NMR. If the combination of protons and neutrons leads to a net spin angular momentum, combined with its charge, the nucleus will posess the characteristics suitable for MRI and is known as an MR active nucleus [5].

There exist many important MR active nuclei, however the one that is most commonly used for MRI is hydrogen. This is due to the fact that the primary composition of most living tissue, including fat and protein, is water (H_2O), which contains two hydrogen atoms per molecule. As a result of this, living or once-living samples have an abundance of MR active hydrogen nuclei and are ideal candidates for achieving detailed MR images. Hydrogen also has the highest gyromagnetic ratio of common nuclei (see Fig.3), resulting in a strong MR signal. The nucleus of a hydrogen atom consists of a single proton, and from this point on, the discussion of MRI will deal solely with proton imaging.

Constants for Selected Nuclei of Biological Interest					
	Nuclear Composition				
Element	Protons	Neutrons	Nuclear Spin, I	Gyromagnetic Ratio β (MHz T^{-1})	% Natural Abundance
^{1}H, Protium	1	0	1/2	42.5774	99.985
^{2}H, Deuterium	1	1	1	6.53896	0.015
^{3}He	2	1	1/2	32.436	0.000138
^{6}Li	3	3	1	6.26613	7.5
^{7}Li	3	4	3/2	16.5483	92.5
^{12}C	6	6	0	0	98.90
^{13}C	6	7	1/2	10.7084	1.10
^{14}N	7	7	1	3.07770	99.634
^{15}N	7	8	1/2	4.3173	0.366
^{16}O	8	8	0	0	99.762
^{17}O	8	9	5/2	5.7743	0.038
^{19}F	9	10	1/2	40.0776	100
^{23}Na	11	12	3/2	11.2686	100
^{31}P	15	16	1/2	17.2514	100
^{129}Xe	54	75	1/2	11.8604	26.4

Figure 3: Table of useful physical propeties for select nuclei used in biological NMR and MRI. (Image from Brown [3].)

2.4 Alignment

At room temperature and with no external magnetic field present, the magnetic moments of hydrogen nuclei are randomly oriented and therefore produce no net magnetization. When placed in an external, static magnetic field $\mathbf{B_0}$, the individual magnetic moments interact with the field tending to align with the field lines as a result of a torque:

$$\boldsymbol{\tau} = \boldsymbol{\mu} \times \mathbf{B_0}. \tag{2}$$

The net alignment of the magnetic moments in a sample produces a polarization within the sample, and is proportional to the applied magnetic field $\mathbf{B_0}$. Due to the two distinct energy configurations of protons, in an applied magnetic field the alignment of the magnetic moments occurs in two directions relative to the field. The lower energy state aligns parallel with the field and the higher energy state antiparallel. The lower of the two energy states is favored and therefore there exists an excess parallel alignment and a net magnetization in the sample, often called the magnetization $\mathbf{M}$ (see Fig. 4).

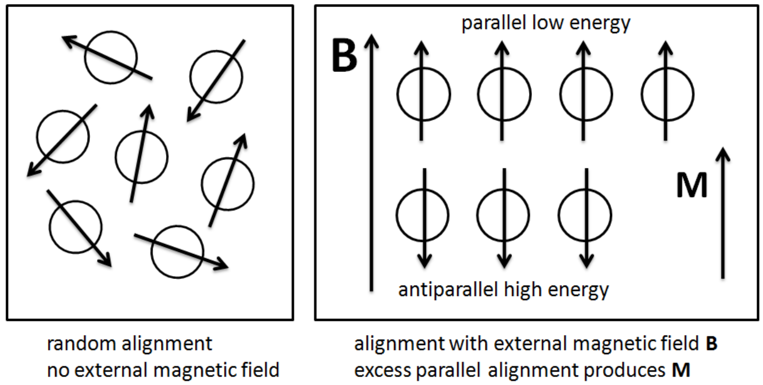

Figure 4: Hydrogen nuclei before and after exposure to an external magnetic field. (Image reproduced from Westbrook [2].)

Once a maximum parallel alignment has been reached, and therefore a maximum $\mathbf{M_0}$, the protons are considered to be at thermal equilibrium. At this equilibrium, the ratio of parallel ($\uparrow$) to antiparallel ($\downarrow$) protons in a sample is given by the Boltzmann distribution. The Boltzmann equation is

$$\frac{N_\uparrow}{N_\downarrow} = \exp\left(\frac{\Delta E}{k_B T}\right), \tag{3}$$

where ΔE is the difference in energy between the parallel and antiparallel states, k_B is the Boltzmann constant, and T is the temperature of the sample in Kelvin. At temperatures at or above room temperature, ΔE is much less than k_BT and Eq. 3 can be written as

$$N_\uparrow - N_\downarrow \approx \frac{\Delta E}{2k_B T} N_p, \tag{4}$$

where N_p is the proton density in the sample. Since $N_\uparrow$ will exceed $N_\downarrow$, the quantity on the left hand side of Eq. 4 is the surplus number of lower energy, parallel protons per unit volume of a sample, referred to as the spin excess. The sum of the magnetic moments of the spin excess protons will produce the magnetization $\mathbf{M_0}$ in the sample. From considerations of classical and quantum mechanics, it has been determined that ΔE is directly proportional to the static magnetic field strength:

$$\Delta E = \hbar \gamma B_0, \tag{5}$$

where $\hbar$ is Planck's constant, γ is the gyromagnetic ratio for protons, and B_0 is the magnetic field strength in units of Tesla (T) or gauss (G) (1 gauss is equal to 10^{-4} Tesla). Any further reference to magnetic field strength will be in units of Tesla, which is more commonly used to describe magnetic field strengths of MRI systems.

2.5 Precession

In the presence of an external magnetic field, protons can be tipped from their alignment producing another type of motion known as precession. This motion results in the magnetic moments of the nuclei outlining a circular path around the field as shown in Fig. 5. An excellent analogy for this is the classic spinning top, which will exhibit a similar motion while spinning about the Earths gravitational field **G**.

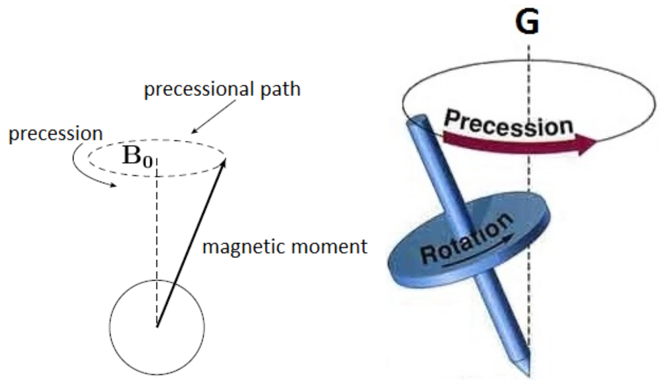

Figure 5: Precession of a hydrogen nucleus compared to a classic spinning top. (Image from Westbrook [5])

The rate of precession of a magnetic moment is called the Larmor frequency, and is given by the Larmor equation:

$$\omega_0 = \gamma B_0 \,, \tag{6}$$

where B_0 is the external field strength, and γ is once again the gyromagnetic ratio of the nucleus in question. The gyromagnetic ratio has units of radians per second per Tesla. Equation 6 can also be written in terms of the precessional frequency as $f_0 = \beta B_0$, where $\beta = \gamma/2\pi$. For protons, β is 42.58 MHz/T which for the operating field of the HSC 7 T scanner corresponds to $f_0 = 298$ MHz.

Within a sample containing many protons, magnetic moments can precess at different phases relative to one another, which refers to the position of the magnetic moments on their precessional path (see Fig. 6). This is due to the different local environments and chemical structures which the protons are a part of, which creates variations in the local magnetic fields, and therefore in the precession frequencies. It is this quality which leads to the ability to perform chemical spectroscopy on a sample containing multiple compounds. The magnetic moments of a group of protons are said to be out of phase if they are at different points on their precessional paths, and in phase when their magnetic moments are all at the same point on their precession.

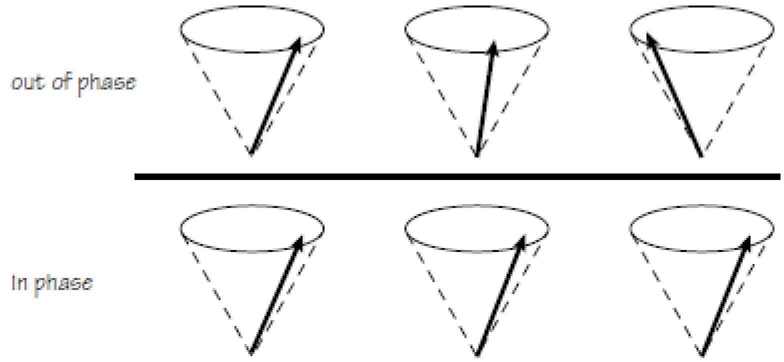

Figure 6: Schematic of 3 nuclear spins in-phase with one another (top), and out-of-phase with one another (bottom). (Image from Westbrook [5].)

2.6 Resonance

In the preceding sections, the proton was described to precess about a magnetic field if its magnetic moment orientation was at some angle relative to the field direction. In a sample containing many protons, as well as other nuclei, interactions exists which cause the motions of the protons magnetic moments to be quite complicated and out of phase. Fortunately, the magnetization vector **M** is much easier to deal with as it is the vector sum of the individual magnetic moments in a unit mass of a sample, and averages out the random motions [6]. Just as the individual magnetic moments, when oriented at some angle relative to an aligning field, will precess around the magnetic field direction at the Larmor frequency, so to will the magnetization vector **M**. It is possible to manipulate the magnetization and change its angle of precession (tip or flip angle) by use of radio frequency (RF) waves which occur at the Larmor frequency, and orthogonal to the aligning field. This manipulation is referred to as resonance, and is the transfer of photons occurring at the same frequency (Larmor frequency) from the RF field to the precessing magnetic moments or magnetization vector **M**.

The RF field responsible for the spin tipping is called the B_1 field, and is produced by RF coils which will be discussed in section 3.3. The tip angle θ of the magnetization in a sample depends on the B_1 field strength as well as its duration t:

$$\begin{aligned} \theta &= \omega_0 t \\ &= \gamma B_1 t. \end{aligned} \tag{7}$$

The process of tipping the magnetization can be observed from the laboratory frame of reference, or from the rotating frame of **M** itself. In the laboratory frame of reference, **M** will acquire a tip angle as it precesses. In the rotating frame, **M** will remain stationary and simply tip downward, as shown in Fig.7.

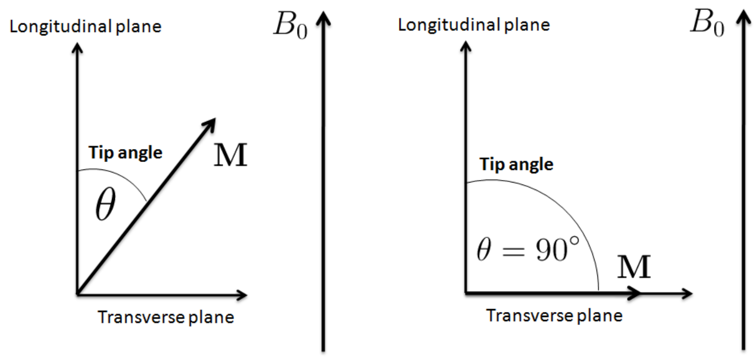

Figure 7: Flip angle of the magnetization $\mathbf{M}$ in the rotating frame of reference. (Image reproduced from Westbrook [2].)

3 MRI Basics

This section describes the basic technique of MRI and the hardware that makes up a scanning system. For further detail of the information presented in this section, please see [1-7].

3.1 B$_0$ Magnets

In the previous sections, the motion of nuclear spins in the presence of an external magnetic field was described. The aligning field is given the name B_0, and is typically the strongest of all magnetic fields used for MR experiments. The magnets which produce the B_0 field are available in a variety field strengths, shapes, and materials. They are generally categorized as low-, medium-, or high-field systems and measured in units of Tesla or gauss. Typically, low-field systems produce field strengths of less than 0.5 T, medium-field systems produce fields between 0.5 T and 1.0 T, high-field systems are in the range of 1.0 T to 3 T [3].

Some B_0 fields are produced by permanent magnets, which are similar to your everyday bar magnet but much more powerful. Many B_0 fields are produced by electromagnets in which an electrical current flowing through a loop of wire will produce the magnetic field. A traditional electromagnet is made of copper wire which has low resistance and allows for easy current flow. The wire is wound in loops and electrically driven with a power supply. As long as there is current present in the windings, the magnetic field is also present. For high-field systems, the B_0 fields are produced using solenoidal superconducting electromagnets made from a niobium-titanium alloy wire immersed in liquid helium. These are very special electromagnets as the niobium-titanium alloy has no resistance to electrical current below a temperature of 20 K. By immersing the electromagnet in liquid helium, which is 4.22 K, it loses all electrical resistance becoming a superconductor. At this point it is possible to pass a tremendous amount of current through the superconductor creating powerful magnetic fields. Because these are superconducting magnets, once a current and consequently a magnetic field is established, they do not decay without raising the temperature of the magnet above 20 K.

Homogeneity or uniformity of the magnetic field is the primary consideration in terms of magnet quality. High homogeneity means that the magnetic field produced will have small variance in field strength over a specified region or volume. This is important, because variation in field strength within the volume of a sample will lead to an inconsistent Larmor precession throughout the sample. This inhomogeneity in field strength will result in nuclei which resonate at different frequencies throughout the sample, and thus reduce the overall magnetization. The homogeneity of a magnet strongly depends on its size and design. Large-bore solenoidal magnets generally produce the most homogeneous fields over large volumes. Short-bore magnets produce smaller regions of homogeneity due to the reduction in magnet windings. Some magnets are designed to be open, and also have reduced regions of homogeneity [3].

3.2 Shim Coils and Gradients

The homogeneity of the B_0 field is extremely important for MRI, and although it is possible to achieve fairly homogeneous fields using a B_0 magnet alone, it is rarely of adequate uniformity. It is possible to correct this using magnetic field producing coils called shim coils, which are a set of coils or metal plates which are embedded within the bore of the main B_0 magnet. Much like you would use a physical shim to slightly adjust the position of an object, shim coils are used to make adjustments to the B_0 field. They are used in instances of inhomogeneous fields, and are capable of reducing these imperfections to achieve a more uniform B_0 field.

Gradient coils, which are used to shim first-order inhomogenieties in the B0 field, also serve another very important purpose in MRI. These coils produce fields that add or subtract from B_0 in a manner that varies linearly with space starting out weak at one point and progressing to a stronger field at another point some distance away. By application of separate gradient fields in the x-, y-, and z-directions, it is possible to control the precise field strength at any point in three dimensional space within the B_0 field. By allowing control of the field strength within the magnet bore, gradient coils allow control of the precession frequency of nuclei at any point in space within a sample. The maximum strength of the gradient fields is an important factor in determining the maximum achievable resolution for imaging, and the speed at which the gradients can be switched on and off is an important factor in determining the maximum scan speed of a system [3].

3.3 Radio Frequency Coils

All MR measurements require a transmit coil to deliver RF pulses responsible for tipping the magnetization within a sample, as well as a receive coil to detect the signals produced by the precessing tipped magnetization [6]. The tipping pulses are magnetic field pulses which oscillate at the Larmor frequency, and are referred to as the B_1 field. RF coils come in a variety of shapes and sizes depending on the type of imaging they are designed for, but a basic RF coil can be constructed using the principles of an LRC (inductance resistance capacitance) circuit.

Suppose we take a piece of conducting wire with some inherent resistance R based on its composition. Now we wrap the wire into a loop and reconnect it back onto itself. If we pass current through the wire, it will create a magnetic field emanating from the isocenter of the loop. We have created an inductor which is capable of storing magnetic energy as described by Ampere's law [14]. The inductance L of this loop of wire is determined by its shape and size, and is measured in units of Henry. Now suppose instead of connecting the two ends of the wire directly onto one another, we place a capacitor C in between the two connecting ends.

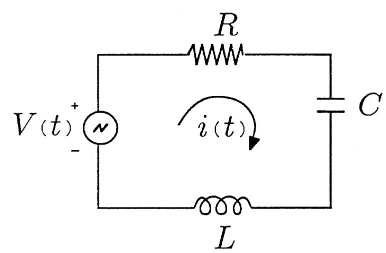

Figure 8: Schematic of an LRC circuit.

We have created an LRC circuit which, when driven by a voltage source, produces an oscillating magnetic field whose angular frequency ω is described by the equation

$$\omega = \frac{1}{\sqrt{LC}}, \tag{8}$$

where L is the inductance of the coil, and C is the capacitance of the capacitor placed between the two ends of the loop of wire.

The signal-to-noise ratio (SNR) is a ratio between the acquired signal in an RF receive coil relative to the total noise of the system. RF coils which are closely fitted with the sample being imaged are able to acheive the highest possible signal, and therefore, a well fitting RF receiving coil will optimize the SNR by acquiring a higher signal, while reducing the noise producing sample volume being "seen" by coil [8]. Since the inception of MRI, numerous RF transmit coil designs have been developed in an attempt to achieve homogeneous B_1 fields at the Larmor frequency. Much consideration has also gone into developing receive coils with high SNR and the ability to receive RF signals of equal gain from any point in the volume of interest.

3.4 Signal Acquisition and Signal-to-Noise Ratio

The precession of the magnetization vector $\mathbf{M_0}$ in the transverse plane resulting from resonance produces a field which passes through a receiver coil. This induces a voltage in the coil, which is the MR signal. Once the RF coil producing the tipping field is turned off, the tip angle of $\mathbf{M_0}$, and most importantly the transverse component of $\mathbf{M_0}$, $\mathbf{M}_\perp$ begins to decrease as the system returns to equilibrium. Therefore the voltage induced in the receiver coil begins to decrease. This signal is called the free induction decay (FID) (shown in Fig.9) because the magnetization is freely rotating, and the induced signal in the receiver coil is decaying with time.

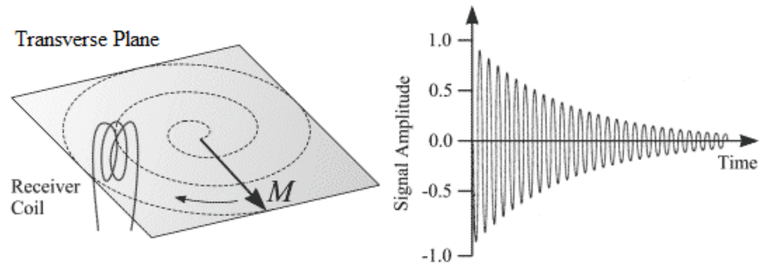

Figure 9: Free induction decay of the net magnetization $\mathbf{M}$. (Image from [4].)

The nuclear magnetic resonance (NMR) signal increases as the square of the Larmor frequency, and because the Larmor frequency is directly proportional to B_0, the signal is proportional to the square of B_0 [9]. Therefore, higher B_0 field strength will produce a stronger signal from a sample. Much of the noise in MRI is due to Johnson noise, which is produced by thermally driven Brownian motion of electrons existing in the receiving coil and also in the sample. In the sample, this noise is caused by randomly varying magnetic fields within (due to random motion of charges) which induce voltages in the RF receiving coil. This type of sample noise increases with higher Larmor frequency and therfore also with field strength [8]. A well designed receiving coil can minimize the interaction with the sample, and reduce the noise produced by electronic motion [10].

3.5 Imaging

At the central point, or isocentre, of the B_0 magnet, the magnetic field is $B_0\hat{\mathbf{z}}$ and the resonant frequency of the protons is ω_0. By application of a linear field gradient $\mathrm{G}_x\hat{\mathbf{z}}$ along the x-direction, say, the resonant frequency will remain at ω_0 at the isocenter, and shift slightly in the directions of increasing and decreasing position x. This results in a magnetic resonance spectrum consisting of more than one signal and is known as frequency encoding. The resonant frequency of the protons will be proportional to their positions in the x-direction:

$$\omega = \gamma(B_0 + xG_x) = \omega_0 + \gamma x G_x \tag{9}$$

$$x = \frac{(\omega - \omega_0)}{\gamma G_x} \tag{10}$$

Adding field gradients in the y- and z-directions will enable 3-dimensional control of the proton precession frequency and phase. By acquiring different signals, it is possible to determine the physical location of the signal production and reconstruct an image using various mathematical techniques. This forms the basis of all magnetic resonance imaging [7].

4 Birdcage Theory

4.1 Field Requirement

The primary requirement for an RF coil is the ability to produce a uniform magnetic field B_1, transverse to B_0 field, and of the form

$$B_1(t) = B_1 e^{i\omega t}, \tag{11}$$

where B_1 is the magnitude of the field and ω is the Larmor frequency. The Larmor frequency is described by

$$\omega = \gamma B_0, \tag{12}$$

where γ is the gyromagnetic ratio for protons. The question is, what kind of current distribution would deliver such a field? Consider an infinitely long cylindrical conductor carrying a z-directed surface current

$$\vec{K} = K_0 \sin(\phi) \hat{z}. \tag{13}$$

It is observed that this current distribution will produce a uniform x-directed magnetic field

$$\vec{B} = \frac{\mu_0 K_0}{2} \hat{x} \tag{14}$$

inside the cylinder [11] as shown in Fig.10.

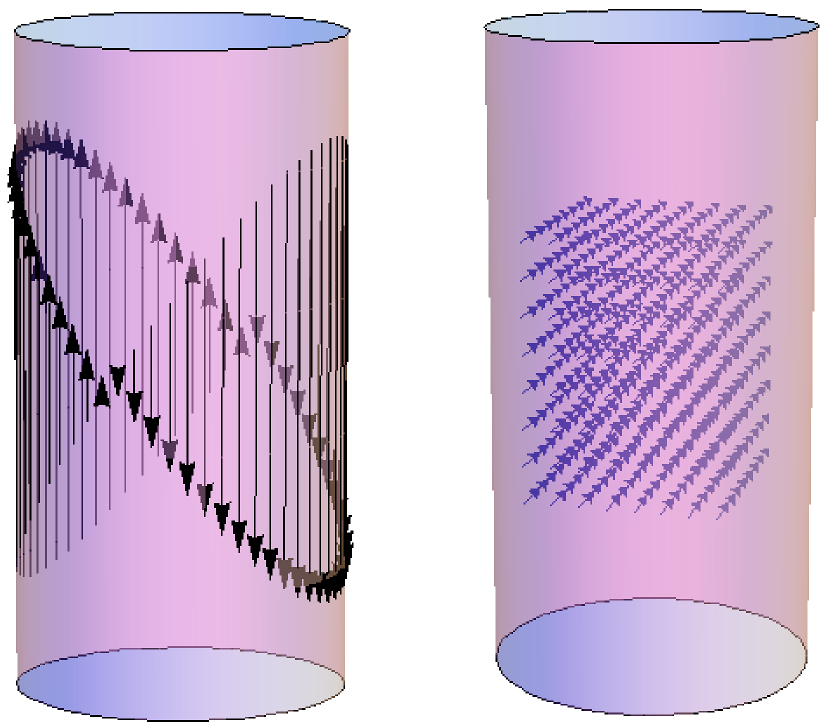

Figure 10: Cylindrical conductor with a surface current $\vec{K} = K_0 \sin(\phi)\hat{z}$ and the uniform magnetic field $\vec{B} = \frac{\mu_0 K_0}{2}\hat{x}$ produced inside the cylinder.

The current flowing in one half of this distribution is

$$\begin{aligned} +I &= \int_0^{\pi} K a d\phi \\ &= K_0 a \int_0^{\pi} \sin\phi \\ &= -2K_0 a, \end{aligned} \tag{15}$$

which can be rearranged to show that

$$|K_0| = \frac{I}{2a}. \tag{16}$$

Substituting this into Eq. 13 gives

$$|K| = \frac{I\sin(\phi)}{2a}, \tag{17}$$

which when substituted into Eq. 14 gives

$$|B| = \frac{\mu_0 I \sin(\phi)}{4a} \tag{18}$$

The sensitivity, or field per unit current of such a current distribution is

$$\tilde{B} = \frac{B}{I} = \frac{\mu_0 \sin(\phi)}{4a} \propto \frac{1}{a}, \tag{19}$$

which shows that as the radius a of the current distribution increases, the sensitivity decreases.

There exist two methods of achieving the sin-ϕ current distribution described above, both of which involve distributing current carrying wires around a cylinder in the z-direction. The first is to distribute the wires of equivalent current amplitude around the cylinder such that the density of the wire distribution follows a sinusoidal pattern. This is shown in Fig. 11.

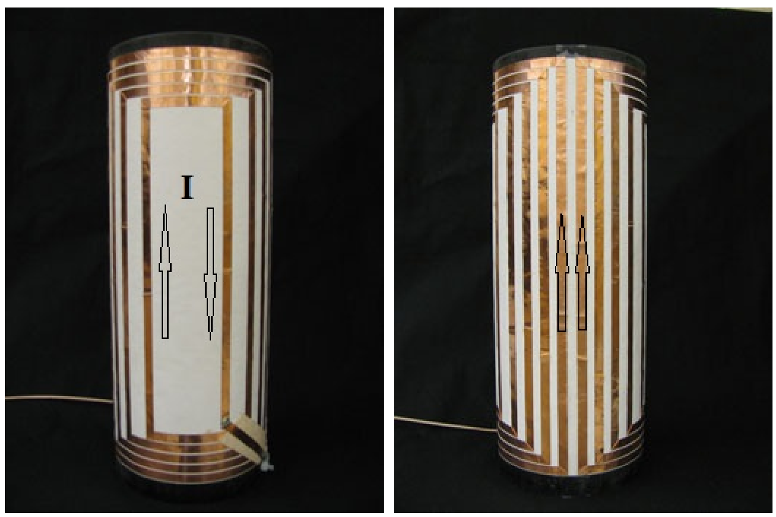

Figure 11: Sinusoidal distribution of wires carrying equivalent current, known as a sin-phi coil. Same coil shown from two angles to display wire distribution. Arrows indicate path of current I.

The second method involves distributing evenly spaced wires around the cylinder, but varying the current amplitude through the wires sinusoidally. This is known as a birdcage design, and will be discussed in section 4.3. The principles of the two methods are summarized here in Fig. 12.

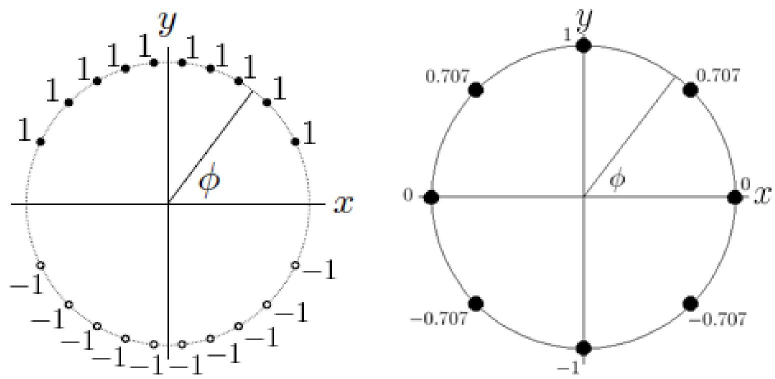

Figure 12: Axial current distribution of the sin-phi coil (left) and the birdcage coil (right). Numbers indicate current magnitude along each wire. (Sin-phi image from Bidinosti [12].)

In either of the two cases, we require that field oscillates at a frequency ω_0 in order to tip the proton spins by an angle θ as described in section 2.6.

4.2 Reciprocity in Signal Strength

The idea of reciprocity relates the magnetic field generated by a coil when current is driven in it, to the induced voltage across the same coil due to an arbitrary, time-varying external magnetic field. Understanding the reciprocity of a receiving coil is very important for obtaining signals from precessing protons within a sample. This is because a precessing magnetization $\mathbf{M_0}$ within a sample behaves like a tiny current carrying loop, and it is very difficult to determine the current induced in the receive coil by the magnetic field produced by this tiny loop. By use of mutual inductance however, the flux cutting through the receive coil produced by the precession of $\mathbf{M_0}$ can be determined mathematically by considering a unit current in the receive coil and determing the field per unit current $\tilde{\mathbf{B}}_1$ which it produces at the point in space where $\mathbf{M_0}$ lies. This works because the mutual inductance between two coils is equal, regardless of which coil carries the currents. The emf ξ induced in the receive coil by $\mathbf{M_0}$ is given by

$$\xi = -\frac{d}{dt}(\tilde{\mathbf{B}}_1 \cdot \mathbf{M_0}), \tag{20}$$

and it can be shown that an RF coil which produces a uniform field through a volume will receive signal from the spins within that volume uniformly [13].

4.3 The Birdcage Resonator

Achieving a uniform field that oscillates at the Larmor frequency ω_0 can be accomplished by means of an RF coil known as a birdcage resonator. Acting as both a transmit coil which can deliver exceptional B_1 field homogeneity over large volumes, as well as a receive coil with high SNR and uniformity, the birdcage resonator has become the most popular of the various designs available. The birdcage is a volume coil which, when excited at two points

90 degrees apart with a phase difference of 90 degrees, generates a circularly polarized B_1 field. Coils of this nature are referred to as quadradrature coils, and compared with a coil producing a linearly polarized field will reduce input power by a factor of two and increase SNR by a factor of $\sqrt{2}$ [11].

The birdcage is cylindrically shaped with evenly spaced, z-directed azimuthally distributed wires around its circumference, end rings connecting these wires, and capacitive elements to create a resonant structure. The birdcage resonator comes in three variations which represent the placement of the capacitive elements. High-pass birdcages have capacitors located on the endrings while low-pass birdcages (see Fig. 13) have capacitors on the legs. Bandpass birdcages have capacitors located on both the endrings and legs. This project deals exclusively with low-pass birdcage resonators, following a previously successful design, and they will be the topic of discussion.

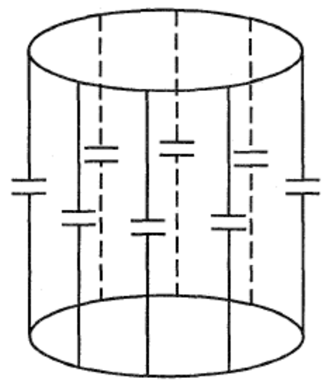

Figure 13: Schematic of an eight-leg, low-pass birdcage resonator. Note that the capacitors are located on the legs of the birdcage structure. (Image from Jin [11].)

When driven at any one point by an oscillating voltage, the birdcage will resonate producing a linear oscillating field inside (shown in Fig. 14). The benefit of the birdcage design is its ability to be driven in quadrature, or at two points 90 degrees apart with a phase difference of 90 degrees. By driving the coil in this manner, it will generate a circularly polarized B_1 field of the form

$$\vec{B}_1(t) = B_1(\cos(\omega t)\hat{x} + \sin(\omega t)\hat{y}), \tag{21}$$

which is shown in Fig. 15.

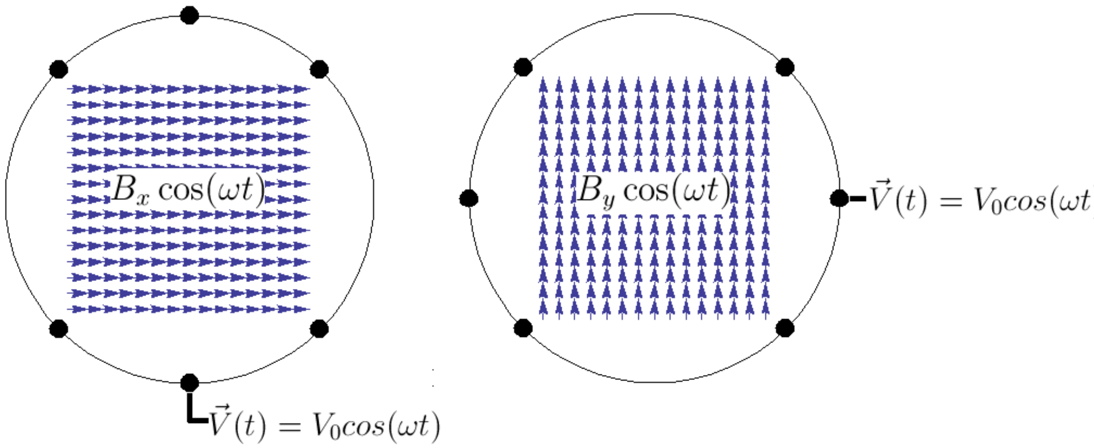

Figure 14: Top view of a birdcage coil being driven at two different points producing linear oscillating magnetic fields in the x- and y-directions.

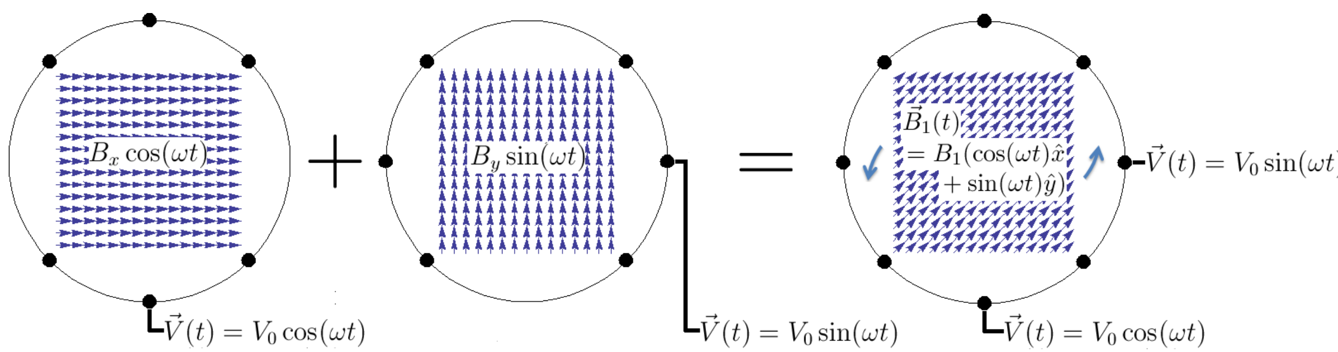

Figure 15: Top view of birdcage coil being driven in quadrature by combining two orthogonal linear birdcage coils.

4.4 Why Quadrature?

Driving a birdcage coil in quadrature has numerous advantages over a single drive point. By creating a circularly polarized field within the volume of the coil, spins are more efficiently tipped when compared to a linear field. This is due to the fact that a linear field will oscillate between its maximum magnitude and zero, only inducing a spin tipping action some of the time. A circularly polarized field however, is continuously at a maximum magnitude and is inducing a tipping torque on the spins through its entire pulse duration. This can be shown by a simple calculation of the magnitude of a circularly polarized field as follows:

$$\begin{aligned} |\vec{B_1}(t)| &= |B_1(\cos(\omega t)\hat{x} + \sin(\omega t)\hat{y})| \\ &= |B_1|(\cos(\omega t)^2 + \sin(\omega t)^2) \\ &= B_1 \end{aligned} \tag{22}$$

As shown in Eq. 22, the magnitude of a circularly polarized field is B_1, and constant with respect to time. This results in tipping which occurs much more rapidly then if the field were linear and only producing the same magnitude of field part of the time, as shown in Figs. 16 and 17.

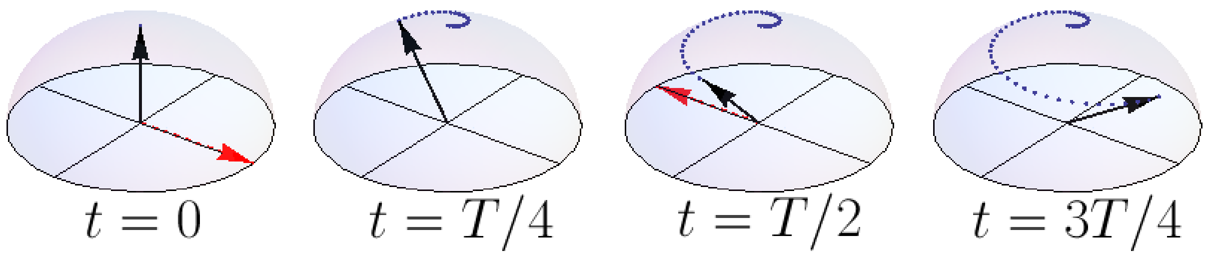

Figure 16: Approximation of spin dynamics of a linear oscillating field in the laboratory frame of reference. Magnetization $\mathbf{M}$ tipping from linear oscillating B_1 field through one period T. Red arrows represent the field $\mathbf{B}_1$, black arrows represent the magnetization $\mathbf{M_0}$. Note the tipping of $\mathbf{M_0}$ as the field oscillates from its maximum amplitude at t = 0 and t = T/2 through its minimum amplitude at t = T/4 and t = 3T/4.

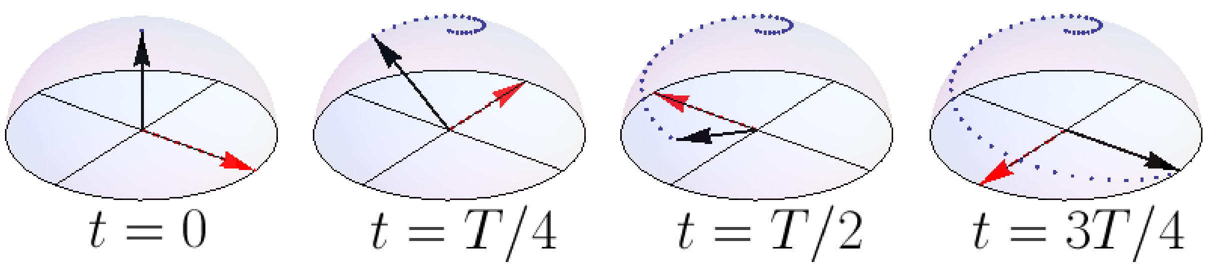

Figure 17: Spin dynamics of a circularly polarized field in the laboratory frame of reference. Red arrows represent the field $\mathbf{B}_1$, black arrows represent the magnetization $\mathbf{M_0}$. Note that field remains at a constant maximum amplitude, and the magnetization is tipped further than with the linear oscillating field in the same time frame.

The quadrature driven birdcage is also considerably more efficient in terms of power consumption. Producing a linear field by driving the birdcage at a single point is inefficient because a linear field can be broken into two opposing circularly polarized fields $\mathbf{B}_1{}^{+}$ and $\mathbf{B}_1{}^{-}$:

$$\mathbf{B}_{linear} = B_1 \cos(\omega t)\hat{x} = \frac{B_1}{2}(\cos(\omega t)\hat{x} + \sin(\omega t)\hat{y}) + \frac{B_1}{2}(\cos(\omega t)\hat{x} - sin(\omega t)\hat{y})\,, \tag{23}$$

where we have defined $\mathbf{B}_1{}^{\pm} = \frac{B_1}{2}(\cos(\omega t)\hat{x} \pm \sin(\omega t)\hat{y})$.

The power consumption of a field producing coil is proportional to the square of the current within it, and the magnitude of the field it produces it proportional to the current within it, therefore, the power consumption is proportional to the square of the field it produces. This argument shows that the power requirement to produce a linearly polarized field is twice that of a circularly polarized field, as shown below.

$$\mathbf{B}_{linear} = \mathbf{B_1}^+ + \mathbf{B_1}^- \tag{24}$$

It can be shown that

$$\bar{P}_{linear} \propto (\bar{\mathbf{B}}_1^+)^2 + (\bar{\mathbf{B}}_1^-)^2 \propto 2(\bar{\mathbf{B}}_1^+)^2 . \tag{25}$$

However, if we apply

$$\mathbf{B_1}^+ = \frac{B_1}{2}(cos(\omega t)\hat{x} + sin(\omega t)\hat{y}) \tag{26}$$

then

$$\bar{P}_{quadrature} \propto (\bar{\mathbf{B}}_1^+)^2 = \frac{1}{2}\bar{P}_{linear}. \tag{27}$$

Another benefit of quadrature coils is that signal-to-noise ratios are enhanced by a factor of $\sqrt{2}$, resulting from the addition of signal from two separate channels, while the noise voltages of each channel remain more or less uncorrelated [8].

5 Birdcage Circuit Basics

As shown in the previous section, a circularly polarized field can be produced by two orthogonal linear fields. In this sense, it is possible to think of an 8-leg birdcage coil, when driven in quadrature, as two orthogonal, 3-loop tuned circuits, as shown in Fig. 18. Each of these circuits forms one of the channels of the birdcage coil, and therefore there are two channels, each producing a linear oscillating magnetic field. Thought of in this way, the channels are independent of each other and each must be tuned to resonate at the Larmor frequency for protons.

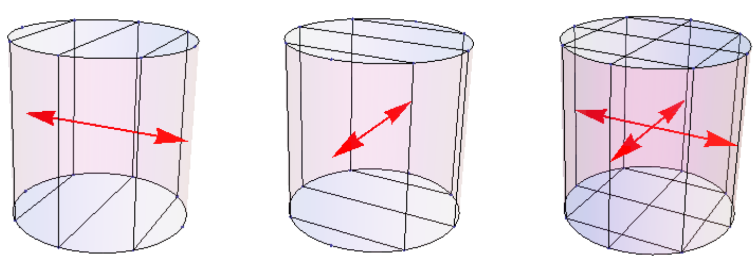

Figure 18: Birdcage structure decomposed into two sets of 3-loop coils, black lines represent oscillating current, red arrows are the uniform magnetic field directions.

5.1 Tuning

It can be observed that each of the birdcages channels behave as a basic LRC circuit. Since each channel must resonate at the Larmor frequency to produce the required oscillating field, the tuning of the entire coil can be naively broken into 2 separate LRC circuits.

The basic LRC circuit is shown in Fig. 8 and described by Eq. 8, where one can see that changing the resonant frequency ω can be achieved by adjusting L or C. With the low-pass birdcage, the overall inductance is set by the geometry of the coil, and therefore it is much easier to adjust the capacitors located at the center of each leg in order to change the resonant frequency ω of each of the channels.

With the particular design used for this project, initial tuning of the birdcage coil itself is performed on the electronics bench by changing the capacitances on each leg, and then fine tuning is performed once the coil is set inside the scanning system and loaded with a sample. The fine tuning is achieved by adjusting the proximity of conducting plates, which are built into the birdcage coil housing, relative to two orthogonal points on the birdcage coil. These plates, or tuning paddles, work by changing the inductance of the birdcage coil in order to adjust the resonant frequency. The change in inductance is related to the magnetic flux in the volume of the coil by

$$L = \frac{\Phi}{I} \tag{28}$$

where Φ is magnetic flux, L is the inductance of the coil, and I is the current in the coil [14]. When the tuning paddle is placed near the coil, eddy currents induced in the paddle by the field of the coil will produce opposing magnetic fields. These induced fields will cancel some of the field within the coil volume, reducing Φ and therefore L as well. By reducing L, the resonant frequency ω will increase as described by Eq. 8. Figure 19 below shows a magnetic field producing solenoid before and after a conducting plate is placed in front of its field lines.

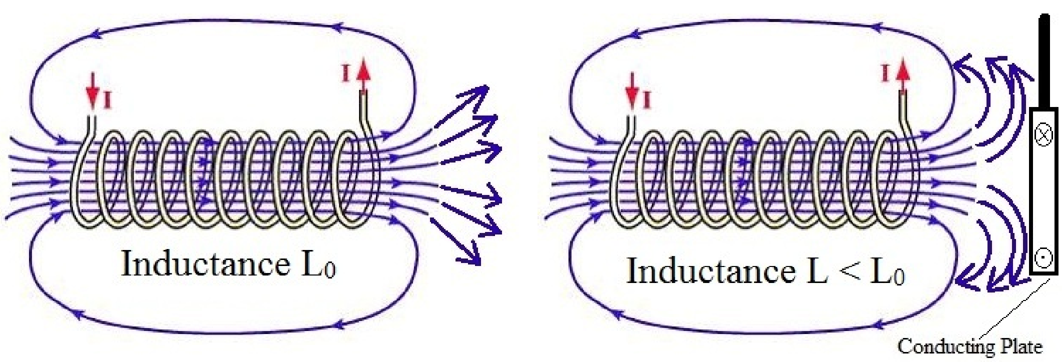

Figure 19: Left:Solenoid with inductance L_0 producing unobstructed field lines. Right:Solenoid field lines being deflected by eddy currents in the conducting plate, inductance of the solenoid is now L $< L_0$.

5.2 Impedance Matching

Impedance matching of electronics is necessary for maximum power transfer from current source to a current load [15]. By matching the input impedance of an electrical load to the output impedance of the current source, power transfer is maximized by minimizing reflections from the load. This can be shown with a simple calculation of a circuit consisting of a voltage V driving a source with impedance Z_S which is connected to a load with impedance Z_L (diagram shown in Fig 20). The power delivered from the source to the load is

$$P_L = \frac{Z_L V^2}{\left(Z_S + Z_L\right)^2}\,. \tag{29}$$

To maximize P_L, which is to say minimize the power reflection, we need to know when the rate of change of the power deliverd to the load relative to the impedance of the load is zero [15].

$$\frac{dP_L}{dZ_L} = Z_S + Z_L - 2Z_L = 0 \tag{30}$$

This is clearly satisfied when $Z_S = Z_L$, which confirms that the impedance of the source must equal the impedance of the load for no power loss between the two.

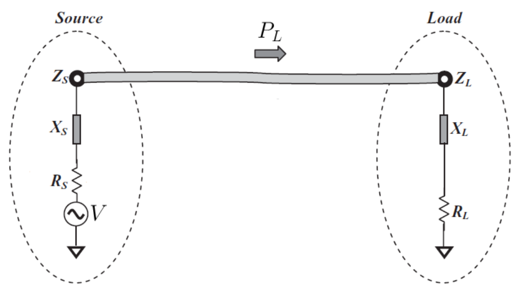

Figure 20: Power delivered from a source with impedance $Z_S = R_S + iX_S$ to a load with impedance $Z_L = R_L + iX_L$. (Image from Li [15].)

For this project, an inductive coupling method is used to transform the impedance into a 50-Ω purely real resistance, full details of which can be found in [16]. Making use of this style of impedance matching requires a special housing to be built which serves to acquire signal from the coil, and also can be easily adjusted to achieve the desired impedance matching for the coil-housing system.

As mentioned previously, an 8-leg birdcage coil when driven in the uniform mode can be thought of as two orthogonal, 3-loop, tuned circuits. Each circuit, or channel, acquires a signal from within the sample volume which must be received independently of the other channel. Making use of a tuned circuit called a matching circuit, the signal from one channel can be converted into a voltage in the matching circuit and adjusted to a 50-Ω real impedance to satisfy the matching requirement of the MRI scanner being used. By capacitively tuning the matching circuit to the same resonant frequency ω_0 as the birdcage coil, and using it to transmit signal via a coaxial cable to the MRI system, the impedance of the birdcage-matching coil system can be adjusted by changing the mutual inductance M_{bm} between the two resonant circuits. This is accomplished by simply changing distance between the birdcage and the matching coil.

The impedance Z of a single channel of the birdcage coil, when coupled with a tuned matching circuit can be described by the equation

$$Z = \frac{{\omega_0}^2 M_{bm}^2}{r_m} = \frac{Q\omega_0 M_{bm}^2}{L_m} = Qk^2\omega_0 L_b\,, \tag{31}$$

where Q is the quality factor of the birdcage, k is the coupling constant between the birdcage and matching coil, and ω_0 is the resonant frequency of the birdcage and matching coil [16]. A circuit schematic is shown in Fig. 22, and Fig. 23 shows a plot of the matching impedance.

The coupling constant k is a proportionality of coupling between the birdcage coil and the matching coil and is described by the equation

$$k = \frac{M_{bm}}{\sqrt{L_b L_m}}, \tag{32}$$

where L_b and L_m are the self-inductances of the birdcage and matching circuits respectively, and M_{bm} is the mutual inductance between the two coils.

The quality factor Q of a resonant circuit can be thought of as the ratio of stored versus dissipative energy of the circuit. The quality factor is described by the equation

$$Q = \frac{\omega_0 L_b}{R_b} \tag{33}$$

where L_b and R_b are the inductance and resistance of the birdcage respectively. Another useful equation which describes Q is

$$Q = \frac{\omega_0}{\Delta\omega}, \tag{34}$$

where $\Delta\omega$ is the full width at half maximum bandwidth of a resonant circuit. This is shown in Fig. 21. The attenuation of the circuit is measured in units of decibel (dB), which in electronics, describes the ratio between two measurements of electrical power [17], and is calculated as follows:

$$dB = 10\log\frac{(Power_1)}{(Power_2)}. \tag{35}$$

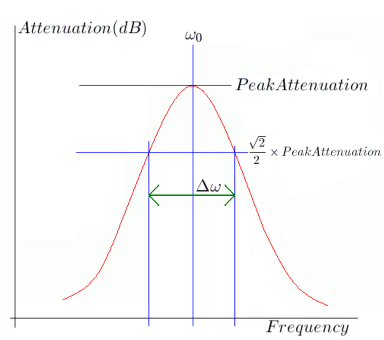

Figure 21: Plot of Q curve for a resonant circuit.

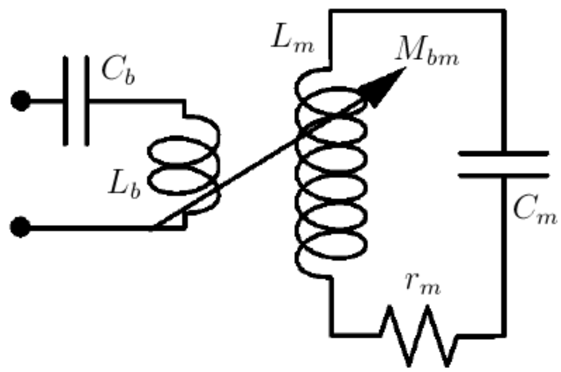

Figure 22: Schematic of tuned matching coil inductively coupled with resonant LRC circuit representing a single channel of the birdcage. (Image from Hoult *et al.* [16].)

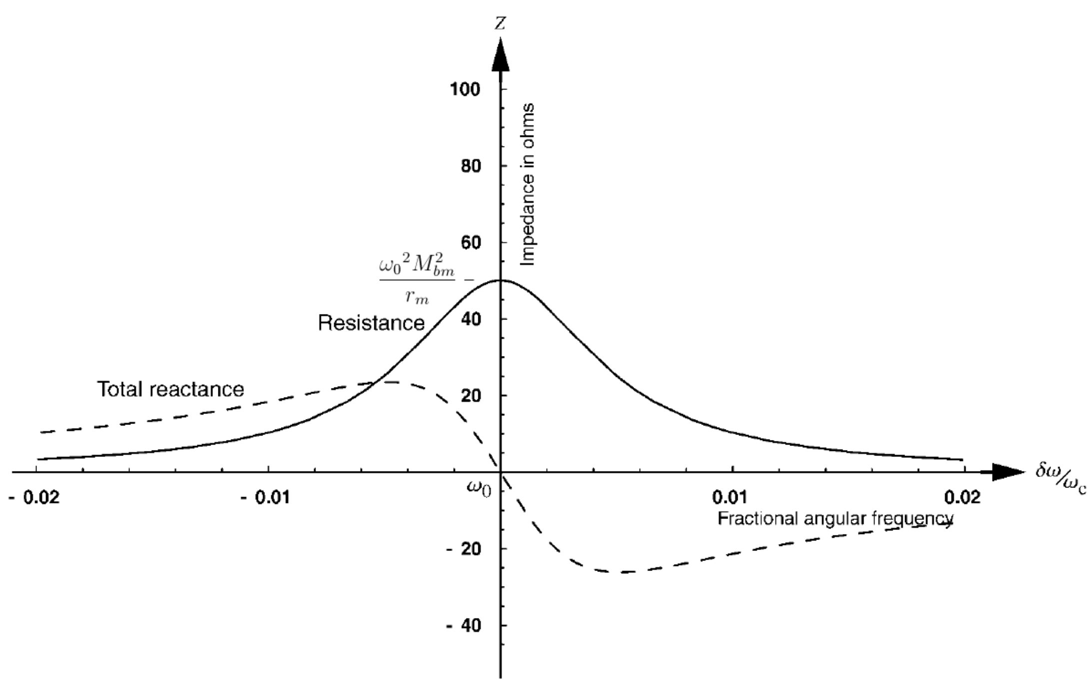

Figure 23: Plot showing the matching system of the circuit in Fig. 22. Note that an impedance of 50-Ω real impedance is achieved when $Z = \frac{{\omega_0}^2 M_{bm}^2}{r_m}$, as described in Eq. 31 (Image from Hoult et al. [16].)

6 Construction

The low-pass birdcage resonator created for this project was constructed and tuned through several steps outlined below. As well as the resonator itself, a housing system featuring magnetic shielding and adjustable tuning and matching was also constructed as part of this project.

6.1 RF Resonator Assembly

The starting point of the resonator was choosing an appropriate base for the birdcage circuitry to be assembled on. It is of extreme importance that former be made from a material which does not produce a strong proton signal itself since it will be subject to the same RF fields as the sample within it. Polycarbonate (PC) is a thermoplastic polymer which, based on its chemical composition, produces very little proton NMR signal. It is also extremely rigid and fairly heat resistant, which allows for easy machining and the ability to solder circuit components in close proximity. For these reasons, PC tubing was chosen as the former on which to assemble the birdcage resonator.

The size of the PC tubing used was determined by the project requirement of delivering a cylindrical sample space 28.5 mm in diameter, suitable for small rodents. PC tubing was ordered from a local plastics manufacturer to meet this specification. The tubing used has an outer diameter of 1.25" (1" = 2.54 cm) with a wall thickness of 0.125", providing the required inner diameter of 1.125" or 28.575 mm. The PC tubing was cut to a length of 2.75", which accommodates a coil of equal length and diameter, as well as the adjustable tuning and matching hardware described in the housing section later on.

The 8 birdcage legs were created using 1/4" adhesive copper tape cut into 1.2" strips and placed about the circumference and along the length of the polycarbonate tube. This was performed by simply determining the circumference of the tube, dividing it into 8 equal segments, and then adhering the copper tape in the 8 leg positions as accurately as possible.

The endrings of the resonator are made from a high-gauge wire as opposed to the same copper tape used for the legs. The reason for this is that the endrings are only present as conductors and not field generators and therefore, using thin wire maximizes the available space on the former. Each of the two endrings were measured and cut to the circumference of the polycarbonate tubing and then soldered to each leg-end and back onto them self forming a connecting circle around the tubing.

Figure 24: Polycarbonate tubing for birdcage former, copper tape for birdcage legs, and conducting wire for birdcage endrings.

After all of the legs and each endring was securely soldered in place, a small segment of tape was removed from the middle of each leg in order accommodate the capacitive elements. In order to determine the required capacitance for each leg, the Penn State Birdcage Builder [18] application was first used to obtain an estimate. This computer program was developed to facilitate birdcage coil design by collecting information about the coil configuration (high-pass, low-pass or band-pass; number of legs; radii of the coil and RF shield; dimensions of legs and endring segments; and desired resonant frequency) and then calculating the leg-capacitance using Kirchoff's current law and lumped circuit analysis.

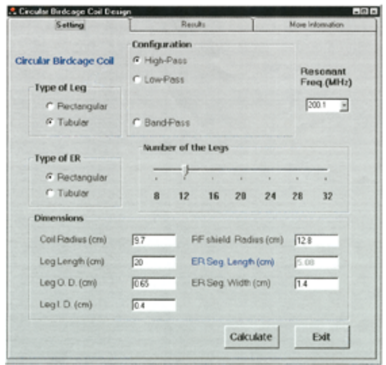

Figure 25: Penn State Birdcage Builder application. (Image from Chin *et al.* [18, 21].)

After inputting the desired resonator parameters into the software, a value of 6.8 pF was suggested for each leg. The suggested 6.8 pF capacitors were soldered into the gaps in the copper tape thus completing the basic birdcage resonator. At this point the resonator is fully functional, however, the values of 6.8 pF given by the application were merely a starting point as they are calculated based on a perfect geometric structure.

Figure 26: Fully constructed birdcage resonator.

6.2 Resonator Tuning

Under ideal circumstances, the resonator would be perfectly symmetric with no imperfections in the circuitry. Being constructed by hand, the symmetry of the resonator is far from perfect and thus the capacitances require slight adjustment to achieve the desired resonance. By means of a set of transmit/receive pickup loops and a network analyzer, it is possible to observe the resonant frequencies of the newly built structure and thereby determine what kind of capacitance adjustments are required. The transmit loop is used to subject the birdcage to a broadband radio frequency field. The birdcage will then produce fields at each of its resonant frequencies or modes, which can be determined using the receive loop. As described in [19] a low-pass birdcage coil will produce n/2 resonant modes, where n is the number of legs on the birdcage. Therefore, an 8-leg lowpass birdcage coil will resonate at 4 specific frequencies.

Figure 27: Broadband sweep of the frequency domain showing birdcage resonant modes.

Shown in Fig. 27 are the four resonant modes of the 8-leg low-pass birdcage coil. It is necessary to adjust the resonant frequencies such that the uniform mode occurs at the Larmor frequency of protons. For the low-pass birdcage structure, the lowest of these resonant frequencies is called the uniform mode as it produces a homogeneous field within the volume of the birdcage [19]. The resonant frequency of an RF coil is based on Eq. 8, which describes a single loop resonator, however, it equally describes each of the two channels of the birdcage circuit. Since the inductance L of the circuit is defined by its geometry, in order to adjust the resonant frequency ω, the capacitance on each leg is changed. According Eq. 8, increasing the capacitance will lower the resonant frequencies and decreasing the capacitance will raise the resonant frequencies. Through several iterations of frequency sweeps and capacitance adjustments, the resonant frequency required is achieved. From the starting capacitance of 6.8 pF on each leg suggested by the Birdcage Builder software, small additions of capacitance were made until the frequency requirement of 300 Mhz was satisfied on each of the channels. The result was that some legs remained at 6.8 pF while others varied from 6.8-11 pF when the birdcage was tuned. Since the birdcage housing will allow for fine tuning adjustments, it is not necessary at this point that the resonant frequency of the coil be absolutely perfect.

6.3 Main Housing Assembly

The housing which contains the birdcage resonator described in the previous section serves several purposes. It provides protection for the birdcage circuitry and shields it from stray RF fields which may be present in the scanning vicinity. More importantly, it drives the birdcage to a resonant frequency and receives the signal acquired by the birdcage using tuned circuits which will be referred to as paddles. Another feature is the inclusion of tuning paddles which allow fine tuning adjustments of the resonant frequency when the coil is placed inside the scanner and loaded with a sample. This is required as inductive coupling between the scanner and the coil, as well as the sample and the coil will shift the resonant frequency. These features will be described later, for now the focus will remain on the construction of the housing. The housing was built in several steps all requiring plastics to be machined using various workshop tools including a lathe, manual mill, computer numerical control (CNC) mill, bandsaw, sander, and a drillpress.

At the core of the housing is a piece of 2 and 6/8 " O.D. PC tubing which was cut to length of 3" using the lathe. The wall thickness of of the tube is 1/8" providing an I.D. of 2 and 5/8". The housing has two endcaps made from high-density polyethylene (HDPE) which hold the body together as well as centers the birdcage (shown in Fig. 28). These were created using a CNC mill and a layout produced in CAD software.

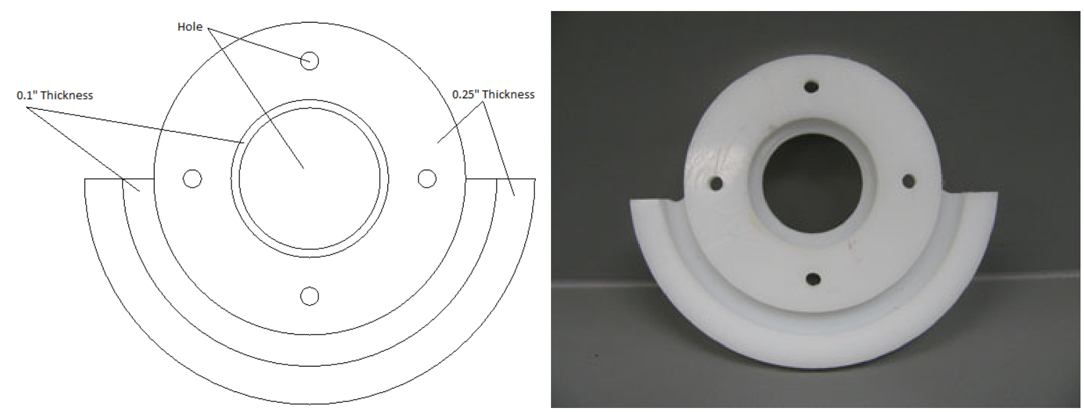

Figure 28: Left: CAD schematic for endcap, Right: Endcap post fabrication.

In order to provide structural support for the housing as well as tracks for the tuning and matching paddles, four Nylatron polyvinyl-chloride (PVC) plastic rods were cut to length. Threaded holes in each end of the rods were created to allow screws to hold the assembly together, and slots were created to provide tracks for the tuning and matching paddles. The entire process was performed using the lathe and manual mill. An HDPE plastic biscuit was created on the lathe to provide further support for the birdcage whichwill rest inside the housing. In retrospect, one of the housing endcaps could have been made to thicker specifications, in which case the biscuit would not have been necessary. Nylon 1/4-20 threaded rod was cut to 1 and 7/8" length on the lathe to fix the tuning and matching paddles described in the following section. The threaded rods, HDPE biscuit, and support rods are shown in Fig. 29.

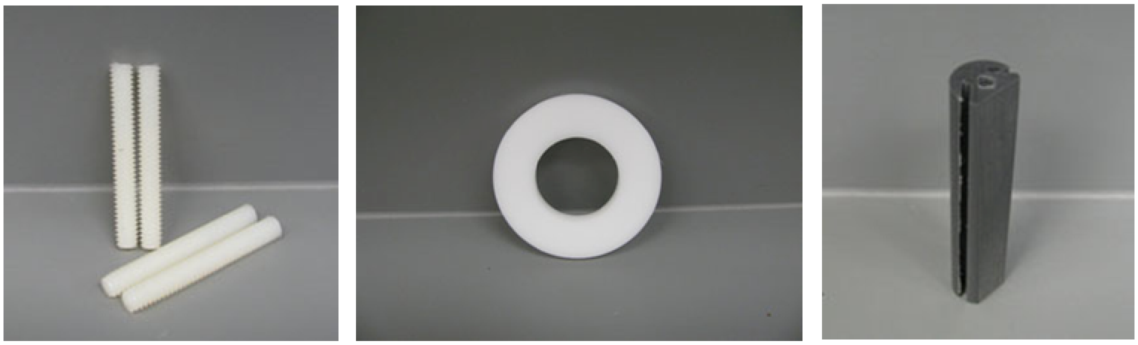

Figure 29: Left: Threaded rods which are attached to the tuning and matching paddles to provide adjustability. Centre: High density polyethylene biscuit. Right: One of four rods which provide structural support as well as tracks for the tuning and matching paddles.

6.4 Tuning and Matching

As mentioned earlier, the housing contains adjustable paddles which serve to fine tune the resonance of the birdcage, as well as adjust the outgoing impedance creating a circuit which is matched to the 50-Ω impedance of the MRI scanner for which this project was designed. Since this birdcage coil will operate in quadrature, there are two sets of tuning and matching paddles in the housing, one for each operating channel.

The tuning paddles, shown in Fig. 30, are simply pieces of copper plated circuit board cut with a shear to 1.35" by 1.35" and then fixed to threaded rods with wire and a screw.

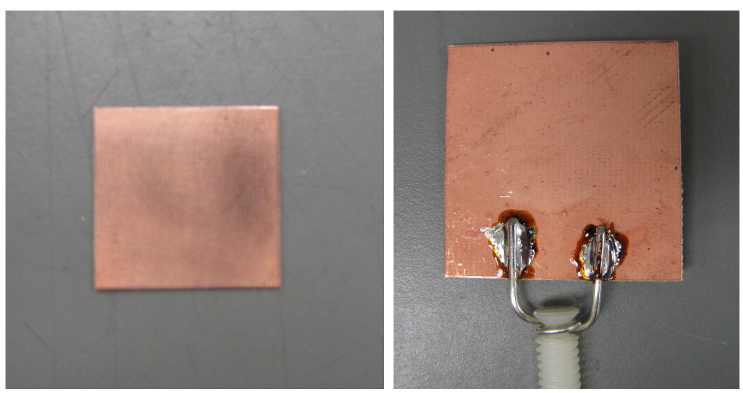

Figure 30: Tuning plate alone and attached to the tuning rod.

The matching paddles, shown in Fig. 31, start off the same as the tuning paddles. A piece of copper plated circuit board cut with a shear to 1.35" by 1.35" is created, and then a square circuit design is drawn on top. Using a sharp blade, the copper plating is cut and peeled away from the board leaving only a square circuit, as well as an edge at the bottom which is used for attaching the paddle to the threaded rod. Cuts in the circuit are created to attach driving wires and provide space for a capacitor to be soldered in, creating a resonant circuit.

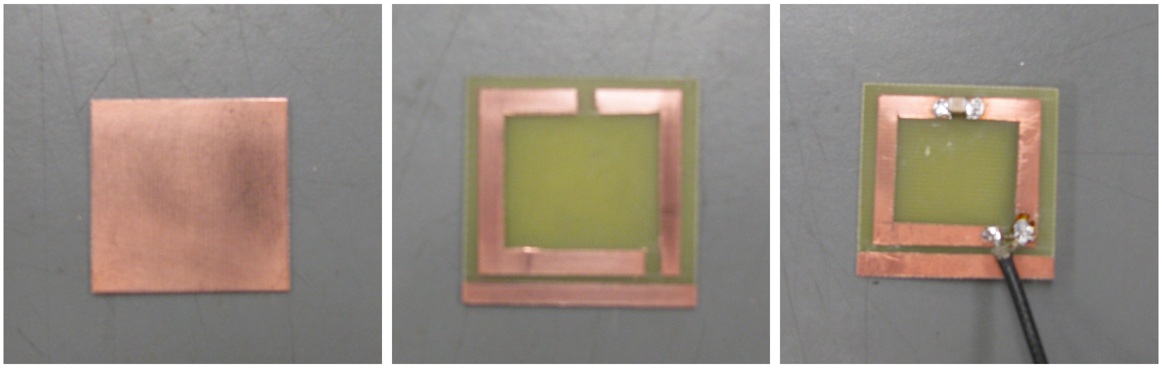

Figure 31: Circuit board before and after the matching circuit is created and tuned.

In order to drive the birdcage and achieve a properly matched circuit, each of the matching paddles must resonate at the same frequency as the uniform mode of the birdcage. Soldering a variable capacitor and driving wires to the paddle to complete the circuit allows it to be connected to a network analyzer and probed for resonance. By adjusting the variable capacitor until the appropriate resonant frequency is achieved, and then measuring the variable capacitor with a multimeter, it can be replaced with a permanent capacitor of equal value. Once this is achieved the circuit will be fixed at a specific resonant frequency when driven by a voltage source. The matching paddle can now be fixed to a threaded rod in the same manner as the tuning paddles.

The two final steps in the housing construction are shielding the birdcage from external fields, and creating a RF choke on the cables which drive the matching paddles. Applying a thin sheet of non-magnetic stainless steel alloy to the exterior of the main housing body provides RF shielding (see Fig. 32). When oscillating magnetic fields impinge on this metallic sheet, eddy currents are induced producing opposing fields that drive out unwanted external noise from the housing, reducing interference.

Figure 32: Main body of housing without and with shielding.

6.5 Cable Traps

Shield currents, or common mode currents are caused by emf generated in the shield of the coaxial cables which connect the RF coil to the MRI system. This results from capacitive coupling which exists between the cable and the various other components such as the shield of the magnetic bore, and leads to unintentional loops in the system inducing voltages. Common mode current is undesirable as it affects coil tuning, image homogeneity, and can cause serious burns to samples within the RF coil [20]. To reduce the common mode current, cable traps can be installed on the coaxial line which drives the RF coil.

The cable trap used for this project is called a floating cable trap, and unlike traditional traps, requires no physical connection to the coaxial cable. Two coaxial concentric conductive cylinders, tuned to the resonance of the RF coil, are wrapped around the signal carrying coaxial cable. This forms a tuned LC tank circuit which creates high impedance to reduce the common mode current at the tuned frequency flowing to the coil [20]. The floating cable trap built is shown in Fig. 33.

Figure 33: Floating radio frequency trap for filtering common mode currents at 300MHz before and after being shrink wrapped.

Once the housing is fully assembled, the tuning and matching rods will be able to screw in and out of the housing allowing the tuning and matching paddles to move into the vicinity of the birdcage coil. By doing so, the resonant frequency and impedance of the corresponding channel on the coil will be adjusted, as described in section 5.1. The fully assembled coil and housing are shown in Fig. 34.

Figure 34: Assembled system before and after the housing body has been attached.

7 Results

7.1 Benchtop Performance Tests

After the birdcage coil was complete, a confirmation of its ability to be tuned to the required frequency and matched to a 50-Ω load was performed using a network analyzer.

Figure 35 shows the network analyzer screen during a tuning and matching procedure. The top left and right windows are set to S11 and S22, respectively, which represent the reflected power for channels 1 and 2 respectively. The dips represents the resonant frequencies of each channel, and the depth of the dips indicate the power reflection, or how well matched each channel is to the 50-Ω load being used. The reflected power is in units of dB and the lower the value, the less reflected power. A reflection value of -30 dB would represent a power loss of 0.1 percent, which is considered an excellent value. Each of the channels are tunable to a resonant frequency of 300 MHz with less than 0.1 percent power loss indicating a successfully tuned and matched coil.

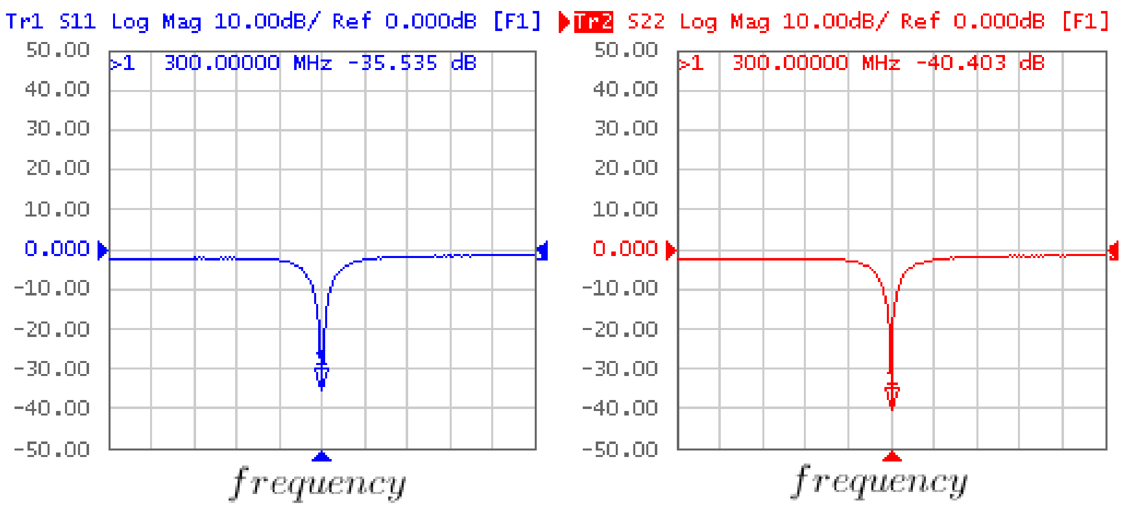

Figure 35: Left:S11 measurement indicating resonant frequency and reflected power of channel 1. Right:S22 measurement indicating resonant frequency and reflected power of channel 2.

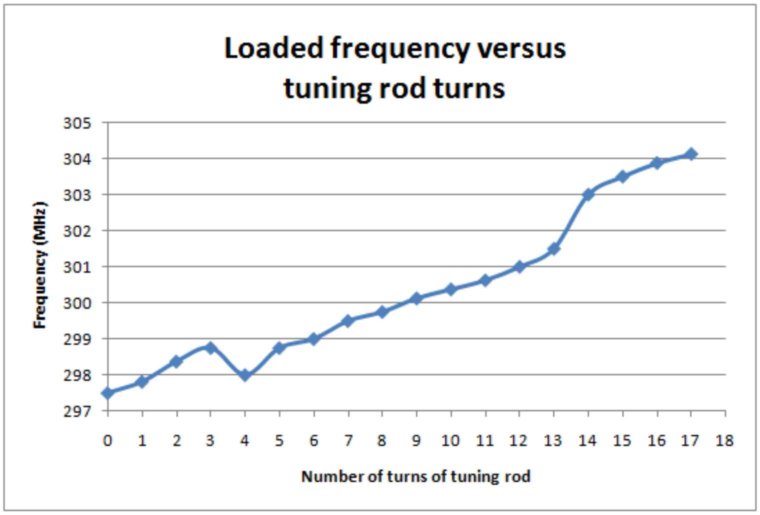

Figure 36: Frequency change of a single channel of the loaded birdcage coil when the corresponding tuning rod is adjusted.

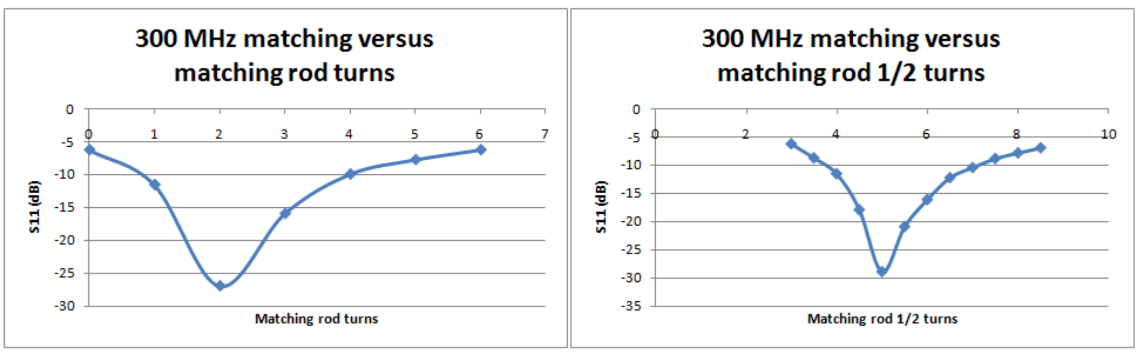

Figure 37: Reflected power change of a single channel of the loaded birdcage coil when the corresponding matching rod is adjusted.

7.2 Test Scans

Testing the performance of the newly constructed 28.5 mm birdcage coil was done using Paravision, an MR-acquisition and processing software developed by Bruker BioSpin. The first set of tests were merely to verify that the coil was working and able to acquire an image. For this, a water based phantom consisting of tap water and $CuSO_4$ was imaged using each of the two channels individually as well as a quadrature combination of the two.

Figure 38: Test images of water based phantom from left to right: channel 1, channel 2, quadrature combination.

As expected, the water sample produced a relatively uniform image for each of the three test scans.

7.3 Comparison of 28.5 mm Coil with 33 mm Coil

After confirming that the coil was functioning correctly, a tissue sample was prepared using an excised rat brain. Once prepared, the sample was placed inside the 28.5 mm birdcage coil, which was then inserted into the MRI magnet bore. The two channels were individually tuned and matched to the system and then connected in quadrature to the MRI system using a device known as a quadrature hybrid. The purpose of the quadrature hybrid is to rephase the two orthogonal channels of the coil in order to combine the acquired signals as described in the theory section. After imaging was performed using the 28.5 mm birdcage coil, another set of images was taken using a 33 mm birdcage coil and the same method.

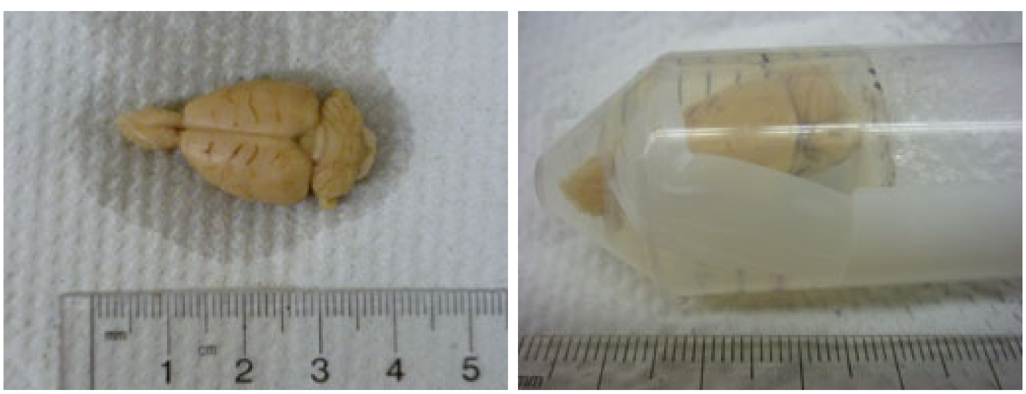

Figure 39: Preparation of excised rat brain for testing purposes.

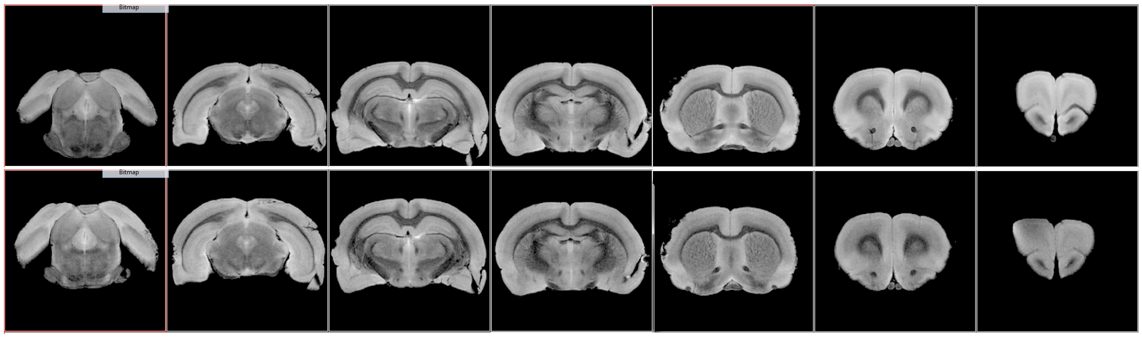

Figure 40: Top: 7-slice scan performed with 28.5 mm birdcage coil and excised rat brain. Bottom: 7-slice scan performed with 33 mm birdcage coil and excised rat brain.

SNR calculations were performed using a Matlab program which takes the mean signal of a region of interest inside the image, and divides it by the standard deviation of the noise in a region outside the image multiplied by 1.5. The division by a factor of 1.5 is a correction to the distribution of backround noise in the image [22]. The 28.5 mm coil yielded an SNR of 30.3 and the 33 mm coil yielded an SNR of 21.7. This indicates that the 28.5 mm coil was capable of delivering an SNR 1.4 times that of the 33 mm coil. It is clear from the SNR comparison as well as the image clarity that the 28.5 mm birdcage coil performed the imaging task much better than the 33 mm coil, as was expected.

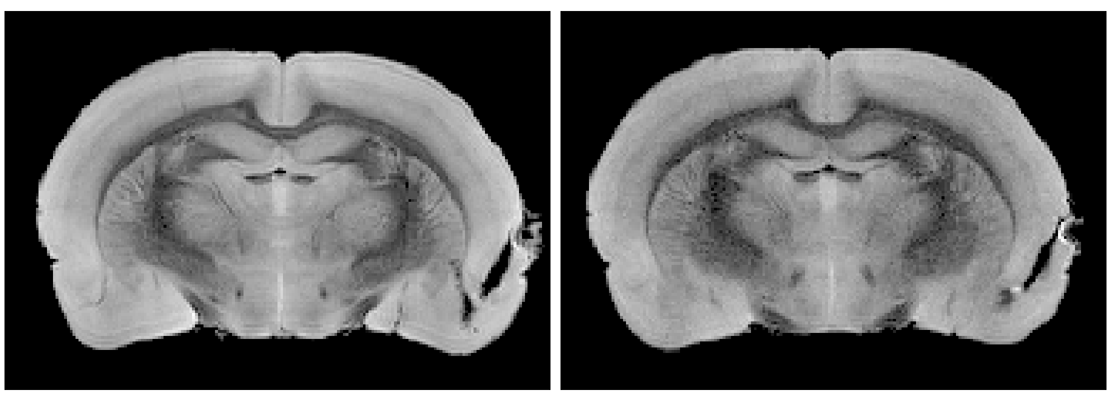

Figure 41: Central slice from the 7-slice imaging sequence for both the 28.5 mm and 33 mm birdcage coils.

7.4 Overnight Scans

One of the main purposes of this project was to achieve an RF coil capable of delivering high quality images of fixed rat brains in order to enhance diagnostic analysis of CNS disorders. The ability to see fine details of brain structure is of particular importance when diagnosing Alzheimer's disease. Changes is brain structure are understood to be notable in the hippocampus of the brain, as described by Dr. Melanie Martin. By performing imaging over longer durations of time, it is possible achieve higher resolution images, resulting in visualization of finer detail in the brain. To test the ability of the newly built 28.5 mm birdcage coil, an overnight scan typical of the type that would be run for research purposes was performed on the rat brain sample shown in the above images. The results were very impressive displaying details to a previously unseen level in the studies performed at the HSC in Winnipeg (see Fig. 42). Especially important is the level of detail displayed in the hippocampus of the brain, which will provide much insight into Alzheimer's studies (see Fig. 43).

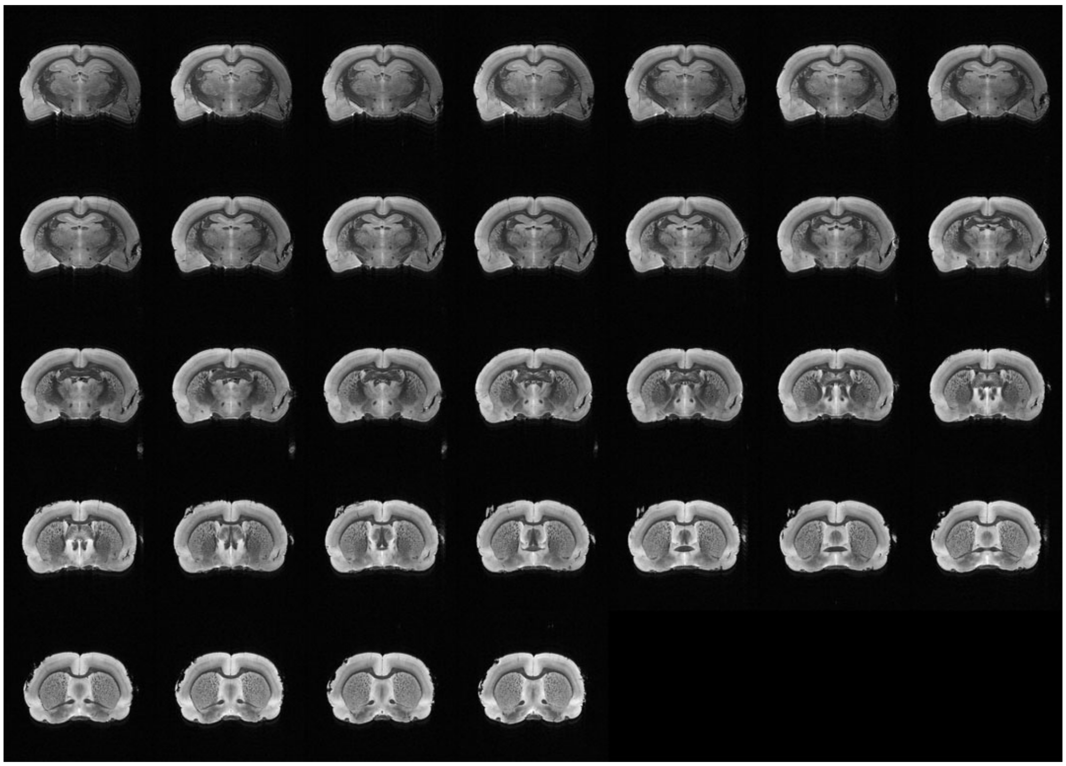

Figure 42: 32-slice overnight image sequence of prepared rat brain.

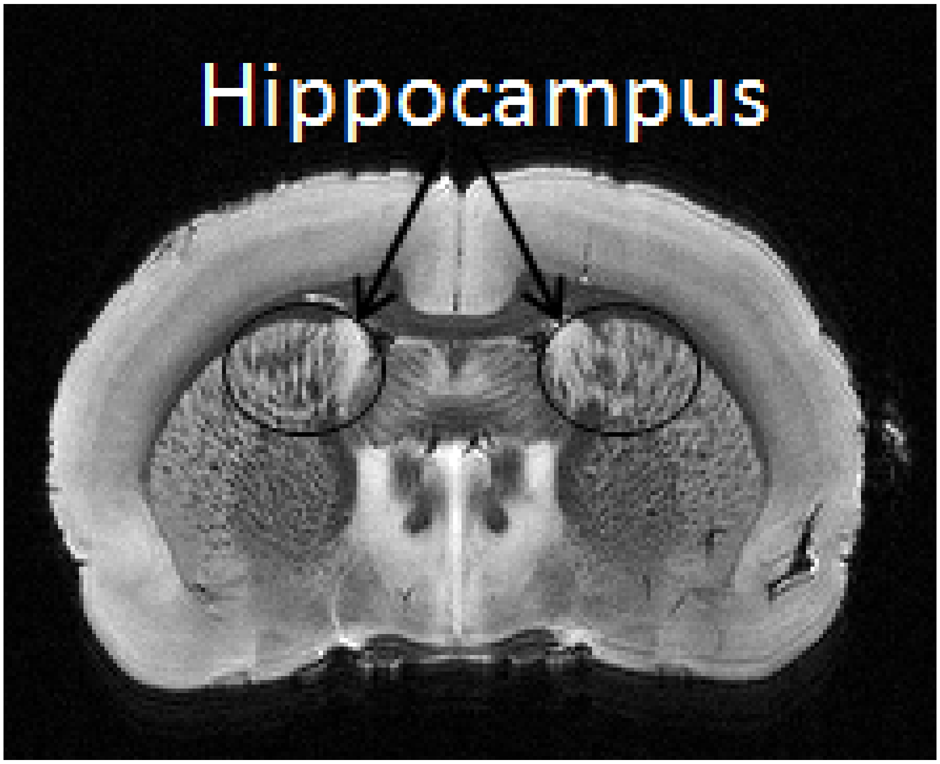

Figure 43: Single image from overnight scan sequence showing high level of detail in the hippocampus of the brain.

8 Conclusion

The goal of building and testing a new 28.5 mm birdcage coil was successfully achieved. The confirmation of image quality improvement when comparing the newly built 28.5 mm birdcage coil to next available size 33 mm birdcage coil reinforces the validity of this project. Using the same prepared rat brain sample in each of the two coils, an SNR improvement of nearly 40 percent was achieved, with significantly increased image detail. By increasing the quality of brain images, finer details can be seen which will lead to better diagnosis of CNS disorders such as Alzheimer's disease and Multiple Sclerosis.

References

[1] Zhi-Pei Lian and Paul C. Lauterbur, Principles of Magnetic Resonance Imaging A Signal Processing Perspective, (IEEE PRESS, 2000).

[2] Catherine Westbrook and Carolyn Kaut, MRI in practice, 2nd edition (Blackwell Science Ltd. , 2000).

[3] Mark A Brown and Richard C. Semelka, MRI-Basic Principles and Applications, (Wiley-Liss, 2003).

[4] http://www.wikidoc.org/index.php/Basic_MRI_Physics

[5] Catherine Westbrook, MRI at a Glance, (Blackwell Science Ltd., 2002).

[6] Hans-J. Smith and Frank N. Ranallo, A non-mathematical approach to basic MRI, (Medical Physics Publishing Corporation, 1989).

[7] Hornak Joseph P. (2011). The Basics of MRI. (http://www.cis.rit.edu/htbooks/mri/index.html)

[8] TW Redpath, Signal-to-noise ratio in MRI, The British Journal of Radiology,**71**, 704–707 (1998).

[9] DI Hoult and RE Richards, The signal-to-noise ratio of the nuclear magnetic resonance experiment, Journal of Magnetic Resonance **24**,71–85 (1976).

[10] TW Redpath and JMS Hutchison, Estimating patient dielectric losses in NMR imagers, Magnetic Resonance Imaging **2**,295–300 (1984).

[11] Jian-Mig Jin, Electromagnetics in Magnetic Resonance Imaging, IEEE Antenna and Propagation Magazine **40(6)**,(1998).

[12] CP Bidinosti, IS Kravchuk and ME Hayden, Active shielding of cylindrical saddle-shaped coils: Application to wire-wound RF coils for very low field NMR and MRI, Journal of Magnetic Resonance **177**, 31–43 (2005).

[13] DI Hoult, The Principle of Reciprocity in Signal Strength Calculations - A Mathematical Guide, Concepts in Magnetic Resonance **12(4)**,173–187 (2000).

[14] David J Griffiths, Introduction to Electrodynamic, 3rd edition (Prentice-Hall inc. 1999).

[15] Richard Chi-Hsi Li, RF Circuit Design, (John Wiley and Sons, 2009).

[16] DI Hoult and B Tomanek, Use of Mutually Inductive Coupling in Probe Design, Concepts in Magnetic Resonance (Magnetic Resonance Engineering) **15(4)**, 262–285 (2002).

[17] Chris Bowick, RF Circuit Design, 2nd edition (Elsevier Inc, 2008).

[18] Chih-Liang Chin, Christopher M Collins, Shizhe Li, Bernard J Dardzinski, Michael B Smith, BirdcageBuilder: Design of Specified-Geometry Birdcage Coils with Desired Current Pattern and Resonant Frequency, Concepts in Magnetic Resonance (Magnetic Resonance Engineering) **15(2)**, 156–163 (2002).

[19] Marc C Leifer, Resonant Modes of the Birdcage Coil, Journal of Magnetic Resonance **124**, 51–60 (1997).

[20] DA Seeber, J Jevtic and A Mennon, Floating Shield Current Suppression trap, Concepts in Magnetic Resonance (Magnetic Resonance Engineering) **21B(1)**, 26–31 (2004).

[21] Penn State Birdcage Builder, (http://med.psu.edu/web/nmrlab/resources/software/javabirdcage)

[22] http://www.revisemri.com/questions/equip_qa/measuring_snr